Spin Relaxation Rates for Mineral Oil and Rubber in Pulsed Nuclear Magnetic Resonance

Anthony Del Valle* and Max N. Frankel†
Department of Physics and Astronomy,
Stony Brook University

(Dated: March 1, 2022)

Abstract:
Nuclear Magnetic Resonance (NMR) has a wide range of applications within medicine, physics, and chemistry. In this experiment, pulsed Nuclear Magnetic Resonance was used to study spin interactions within samples of mineral oil and rubber in a constant external magnetic field. Applied radio-frequency pulses perturbed the sample's nuclear spins in order to observe the rate at which they realigned with the external field. Transverse and longitudinal relaxation rates were recorded and used to characterize the inhomogeneity of the external magnetic field and spin interactions within the sample.

I. INTRODUCTION:

The technique of NMR was first used by Isidor Isaac Rabi to determine the magnitude and orientation of nuclear spin of atoms in an atomic beam [1]. Rabi was awarded the Nobel Prize in 1944 for his work with NMR. NMR was further developed by Bloch, Packard and Hansen at Stanford University [2], as well as Purcell, Torrey, and Pound at Harvard University [3]. In his work, Bloch developed a geometrical representation for the orientation of magnetization vectors in an oscillating external field, known as the Bloch Sphere [4]. The Bloch sphere is important in several subfields of physics, ranging from condensed matter theory to atomic physics and optics. For instance, this diagram plays a vital role in Quantum Computing as a representation for single-photon qubits [5], and is widely used to describe two level systems in atomic physics [6]. Additionally, out of Rabi's work, a technique very similar to NMR was developed by Norman Ramsey, which is now used as the basis for timekeeping with atomic clocks [7].

NMR is a technique which involves observing the spins of a given material in a magnetic field and subjecting them to radio-frequency pulses which typically come in $\frac{\pi}{2}$ and π pulses. These are named after the orientation which they apply on the standard vector which is pointing in the direction of the magnetic field. The Bloch vector is used to represent the average spin orientation of all of the individual nuclei within our given sample. Typically, we represent the standard vector as being in either a rotating reference frame or a lab reference frame, which are visually described on the Bloch Sphere, as shown in Fig 1. The purpose of these reference frames is to simplify the visualization of the magnetization vector as it processes along a certain orientation.

Nuclear Magnetic Resonance (NMR) is used medicine and chemistry for techniques such as NMR spectroscopy, which is a technique used to identify the molecular composition of an unknown sample. This is possible due to each sample reacting to an external magnetic field in a different manner. Subsequently, this identification is also used within medicine as a technique to understand chemicals better and help researchers develop more effective drugs [8]. In the last decade, the technique of NMR spectroscopy has been further developed through the use of diamond nitrogen vacancy centers [9].

II. THEORETICAL MODEL

A. Larmor Precession

A sample composed of a collection of nuclear spins with magnetization vector $\vec{M}$ in an external magnetic field $\vec{B_0}$ experiences a torque

$$\vec{\tau} = \gamma(\vec{M} \times \vec{B}) \tag{1}$$

where γ is the gyromagnetic ratio. This causes the sample's magnetization vector to precess at constant magnitude around the direction of $\vec{B_0}$ at the Larmor frequency [10].

$$\omega = \gamma B_0 \tag{2}$$

By convention, let the external magnetic field point in the $\hat{z}$ direction.

$$\vec{B_0} = B_0 \hat{z}$$

* anthony.delvalle@stonybrook.edu
† max.frankel@stonybrook.edu

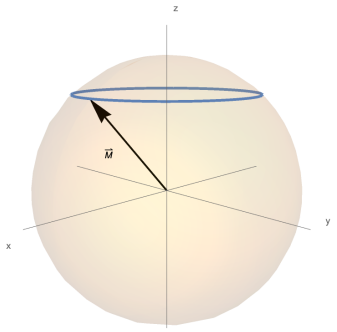

FIG. 1. Diagram showing the precession of $\vec{M}$ on the Bloch Sphere around the external field $\vec{B_0}$ pointing in the $\hat{z}$ direction

B. RF Pulses

Suppose that a sample starts with its magnetization vector parallel to the external field $\vec{B_0}$, as is the case in thermal equilibrium. Now suppose that an oscillating magnetic field with magnitude much less than the external field and frequency equal to the Larmor frequency $\omega = \gamma B_0$ is applied along the x axis. In a particular rotating reference frame, it can be shown that the oscillating field causes the the magnetization vector to rotate at constant angular velocity along a line of longitude on the Bloch Sphere [11].

We refer to pulsing the oscillating magnetic field as a radio frequency (RF) pulse. By pulsing the oscillating magnetic field on for some time, the magnetization vector will have rotated away from the north pole of the Bloch Sphere. Applying an RF pulse for the time in which the angle between $\vec{M}$ and $\hat{z}$ grows to $\pi/2$ is referred to as a $\pi/2$ pulse. Applying a pulse for twice the duration is referred to as a π pulse, as it changes the angle between $\vec{M}$ and $\hat{z}$ to π.

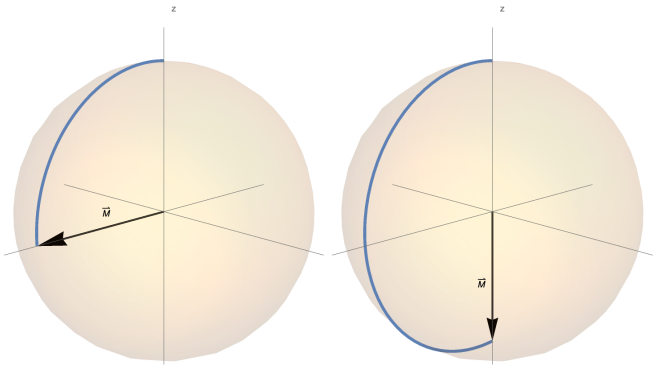

FIG. 2. $\pi/2$ (left) and π (right) pulses on the Bloch Sphere in a rotating reference frame

C. Longitudinal Relaxation Time

Suppose, now, that a $\pi/2$ pulse is applied to a sample in thermal equilibrium, bringing its magnetization $\vec{M}$ from the north pole of the Bloch Sphere to the xy plane of the laboratory reference frame, where it precesses. From Eq. 1, it appears that the magnetization should precess indefinitely. In experiment, however, the magnetization relaxes back to alignment with the external magnetic field, $\vec{B_0}$. This relaxation is due to interactions between each nuclear spin, the spin of its electrons, its neighbor spins, and thermal agitation. Bloch modeled the relaxation rate of $\vec{M}$ back to alignment with $\hat{z}$ as an exponential decay that occurs in characteristic time T_1

$$\frac{dM_z}{dt} = \frac{M_0 - M_z}{T_1}$$

where M_z is the component of $\vec{M}$ in the $\hat{z}$ direction and M_0 is the magnitude of $\vec{M}$ in thermal equilibrium [10].

Let $t = 0$ be the time immediately after a π pulse has been applied, such that $M(0) = -M_0$. It follows that

$$M_z(t) = M_0\left(1 - 2\exp\left(-\frac{t}{T_1}\right)\right) \tag{3}$$

D. Transverse relaxation time

Suppose a $\pi/2$ pulse is again applied to a sample in thermal equilibrium. The relaxation of the transverse component from its maximum value M_0 back to 0, when $\vec{M}$ is parallel to $\hat{z}$, is similarly modeled to be exponential decay. However, this decay occurs in a different characteristic time T_2 than the longitudinal relaxation, which occurs in T_1.

$$M_\perp(t) = M_0\left(\exp\frac{-t}{T_2}\right) \tag{4}$$

The transverse and longitudinal relaxation times differ for two main reasons: inhomogeneity in the magnetic field and spin interactions.

First, we will discuss dephasing due to magnetic field inhomogeneity. In Eq. 2, $\vec{B}$ was assumed to be uniform across the sample. In practice, the external magnetic field will have some slight degree of inhomogeneity, causing ω to vary across the sample.

The magnetization vector is the sum of the nuclear spins in the sample. If the local magnetic field differs between nuclei, their spins will precess at different frequencies. This causes the spins to dephase as they precess along their path of constant latitude on the Bloch Sphere.

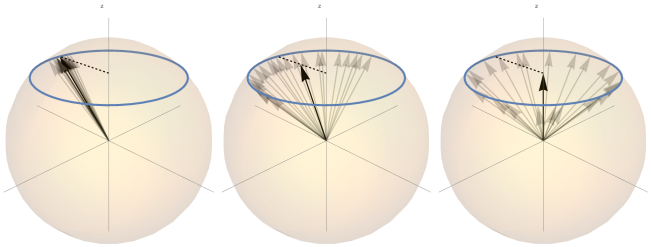

FIG. 3. Even if T_1 is infinite, the transverse component of the magnetization vector will approach zero if there is inhomogeneity in the external magnetic field. The three spheres show how the individual spins, shown as transparent vectors, might dephase from their initial coherent state over time in a rotating reference frame. Their sum is the magnetization, depicted as the opaque vector. Note that the length of the individual spin vectors has been scaled up for comparison with the magnetization vector.

The characteristic time in which dephasing occurs is referred to as T_2^*. We thus split T_2 into two components

$$\frac{1}{T_2} = \frac{1}{T_2^*} + \frac{1}{T_2'} \tag{5}$$

where T_2' is the relaxation rate due to spin interactions with their neighbors and with the rest of the sample as well as thermal agitations. As discussed earlier, the characteristic time for relaxation after a π pulse due to thermal agitations is T_1. Thus, letting T_2" be the characteristic time for relaxation due to spin-spin interactions, the relaxation time due to spin interactions for the transverse component of $\vec{M}$ after a $\pi/2$ pulse is

$$\frac{1}{T_2'} = \frac{1}{T_2"} + \frac{1}{2T_1}$$

Thus, T_1 and T_2' contain information about the rate of relaxation due to thermal effects and spin interactions, respectively, and T_2^* contains information about the inhomogeneity of the external magnetic field. T_1 and T_2' depend on the chemical composition of a sample, and thus their measurement can be used to characterize a sample.

III. EXPERIMENTAL SETUP

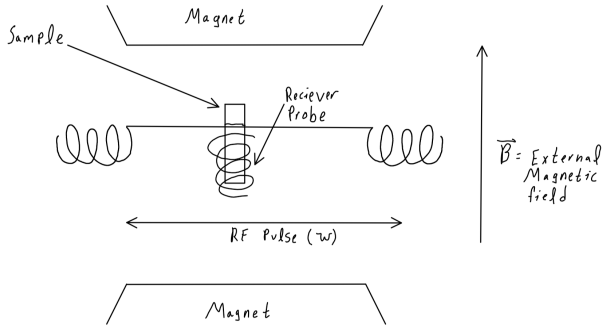

FIG. 4. A hand-drawn scheme of the direction of the magnetic field, along with the receiver probe and the direction of the radio-frequency pulse with angular frequency ω

For this setup, a signal is generated by pulse programmer which is sends a pulse through an RF synthesized oscillator and amplifier. This RF pulse is then sent through a magnetic apparatus. The main component of this is a large magnet which serves to align the bulk magnetization vector in one uniform direction. Subsequently, the magnetization is subject to the RF pulse which comes in two forms, a $\frac{\pi}{2}$ pulse and a π pulse (See Sec. II) which alter the bulk magnetization vector. From here, the motion of the magnetization is detected by 2 different detectors. One is a RF amplitude detector which has an output proportioned to the peak amplitude of the RF precession signal. The second one is a mixer which shows the difference between the pulse sent through the RF oscillator and the received signal. This is sent through a RF detector and displayed on our oscilloscope as channel 1. This mixer uses the following equation to determine the difference between the frequencies when $\omega_1 \approx \omega_2$.

$$sin(\omega_1 t) * sin(\omega_2 t) = \frac{[cos(\omega_1 - \omega_2)t - cos(\omega_1 + \omega_2)t]}{2} \tag{6}$$

Additionally, there is a continuous wave frequency which is generated by the RF synthesized oscillator and sent directly to a mixer which displays on the oscilloscope as channel 2. The receiver is able to detect certain orientations of the magnetization vector, which abide by the Bloch Equations. This allows us to determine the relaxation time associated with different components of the vector. As stated in Sec I, the relaxation times are different for every material tested, which allows them to be characterized by a unique relaxation time. For a formal review of the equipment which was used in this process, observe the list below:

1. GW INSTEK GDS-1102A-U
2. Varian Associates V2901 Regulated Magnet Power Supply

3. TeachSpin 15 MHz Reciever, Pulse Programmer , 15 MHz OSC/AMP/MIXER

4. Keithly 179A TRMS multimeter

Data was collected using the oscilloscope's detailed mode, which records a set of 4000 data points with an accuracy of $\pm(3\% * |Readout| + 1mV + 1div)$ in voltage and $\pm 0.01\%$ in time [12]. The data was exported as a CSV file and fitted to a theoretical model using Mathematica's NonlinearModelFit function. We were able to ensure that our fit was accurate by using a reduced χ^2 fit in order to test our results.

$$\chi^2 = \sum_{i=1}^{n} \frac{(O_i - C_i)^2}{\sigma_i^2} \tag{7}$$

From here, we used our results to obtain the χ^2 per degree of freedom.

$$\chi_v^2 = \frac{\chi^2}{n - m} \tag{8}$$

Where O_i = Observed data , C_i = Calculated data, n = number of data points, and m = degrees of freedom.

IV. MEASUREMENTS

A. Calibration

1. Finding resonance $\omega_{RF} = \omega$

The model of $\pi/2$ and π pulses discussed in Sec II B required that the RF frequency be equivalent to the precession frequency of $\vec{M}$ around $\hat{z}$, ω. As discussed in Sec II D, the Larmor frequency varies across any given sample due to inhomogeneities of the magnetic field. Because the magnetization vector $\vec{M}$ is the sum of the nuclear spins across the sample, the precession frequency ω of $\vec{M}$ is the mean frequency of the distribution of precession frequencies of the collection of nuclear spins in the sample.

In the experimental setup, the mixer outputs a signal with frequency equal to the difference between the RF pulse frequency ω_{RF} and the magnetization vector's precession frequency ω. Before using pulse sequences to take measurements of the different relaxation times, the frequency of the RF pulse was adjusted until no oscillations were seen in the mixer signal, indicating that $\omega_{RF} \approx \omega$.

2. Creating $\pi/2, \pi$ pulses

In the experimental setup, channel 1 of the scope recorded the envelope of the receiver voltage signal, which was proportional to the magnitude of the transverse component of $\vec{M}$, $M_\perp(t)$, after a $\pi/2$ pulse, referred to as the Free Induction Decay (FID). As seen in Fig 2, after a $\pi/2$ pulse, the transverse component of the magnetization vector should be at a maximum, while after a π pulse, it should be at a minimum.

In order to create a $\pi/2$ pulse, the pulse length was increased on the TeachSpin apparatus from 0 until the amplitude of the FID signal reached a local maximum for the first time. To create a π pulse, the pulse length was increased until the amplitude of the FID signal passed its first maximum and reached a local minimum.

B. Data acquisition

1. Accuracy of measurements

There were several sources of uncertainty in this measurement. To start, the oscilloscope accuracy, listed in the manufacturer's manual, was $\pm 3\% * |Readout| + 0.1div + 1mV$ in voltage and $\pm 0.1\%$ in time [12].

The signal measured by channel 1 of the oscilloscope also had noise with a standard deviation of $0.03mV$, measured about some background level, as seen in Fig. 5.

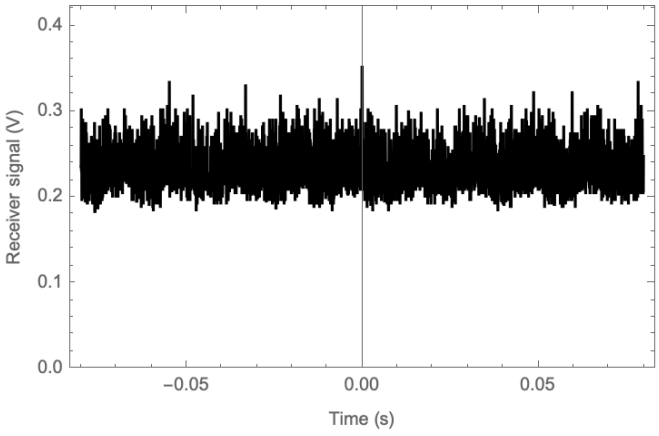

FIG. 5. Receiver signal in the absence of pulses, showing a clear offset of the background signal

Additionally, in the presence of pulses, the peaks in the oscilloscope data fluctuated. The fluctuation was approximately the same for each measurement for both mineral oil and rubber, and was estimated visually using the oscilloscope to be $\pm 300mV$. This uncertainty was the greatest of the three sources mentioned thus far, and therefore was used as the error bar in voltage for each raw data point. The uncertainty in time was taken to be that specified by the manufacturer's manual.

2. Measurement of T_2

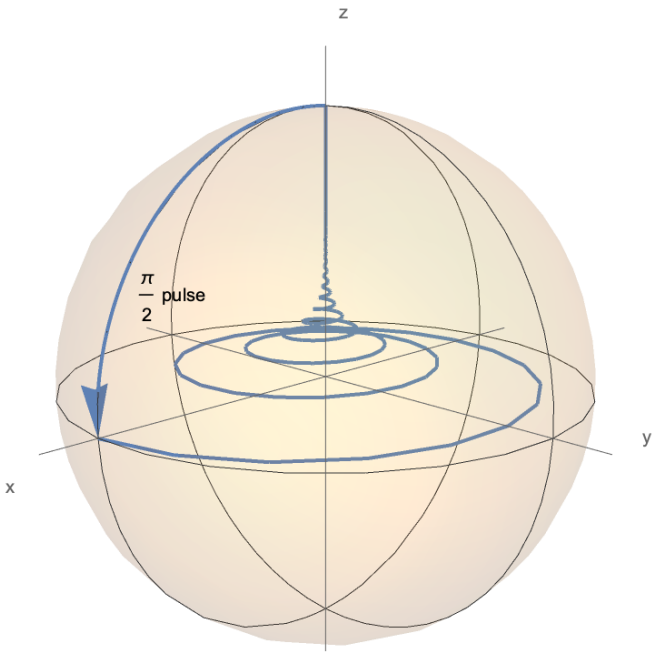

FIG. 6. Simulation of the relaxation of $\vec{M}(t)$ as it precesses about the $\hat{z}$ axis at some arbitrary frequency ω after a $\pi/2$ pulse is applied to a sample in thermal equilibrium, using Eq. 3 and Eq. 4 with some arbitrary T_1 and T_2 such that $T_1/T_2 = 10$.

T_2 is defined to be the relaxation time of $M_\perp(t)$ after a $\pi/2$ pulse, which is simply the FID signal. To calculate T_2, the FID signal was measured with channel 1 of the scope. As shown in Eq. 4, the expected FID signal after a $\pi/2$ pulse is simply exponential decay.

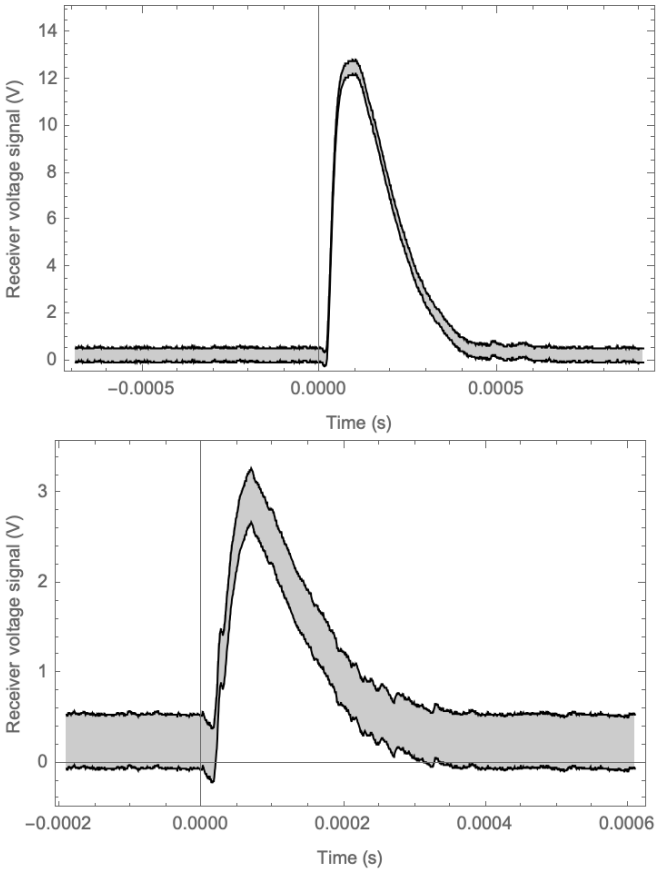

FIG. 7. Confidence interval for FID signal after a $\pi/2$ pulse recorded for mineral oil (top) and rubber (bottom) used to calculate T_2 for the respective samples

As seen in Fig 7, after the FID signal reaches is maximum value from the $\pi/2$ pulse, it did indeed decay exponentially. In order to calculate T_2, the data after the peak amplitude was fitted to Eq. 4.

3. Measurement of T_2'

As seen from Eq. 5, if the effects of T_2^* were removed, the transverse relaxation time T_2 would be equal to T_2'. While there is no way to completely remove the dephasing effects of the inhomogeneous field, there is a simple way to reverse them.

Suppose that a $\pi/2$ pulse is applied to a sample with an infinite T_1. After some time, the individual spins dephase due to the differing local magnetic fields at each nucleus causing different precession rates. Applying a π pulse some time $\tau/2$ after the $\pi/2$ pulse rotates each spin by angle π around the vector representing the RF pulse in the rotating frame. Because the spins must still precess in the same direction, if the magnetic field is constant over time, the dephasing of the spins will be reversed $\tau/2$ seconds after the π pulse. The moment where the spins come back together, temporarily restoring coherence and causing a peak in $M_\perp$, is known as a spin echo.

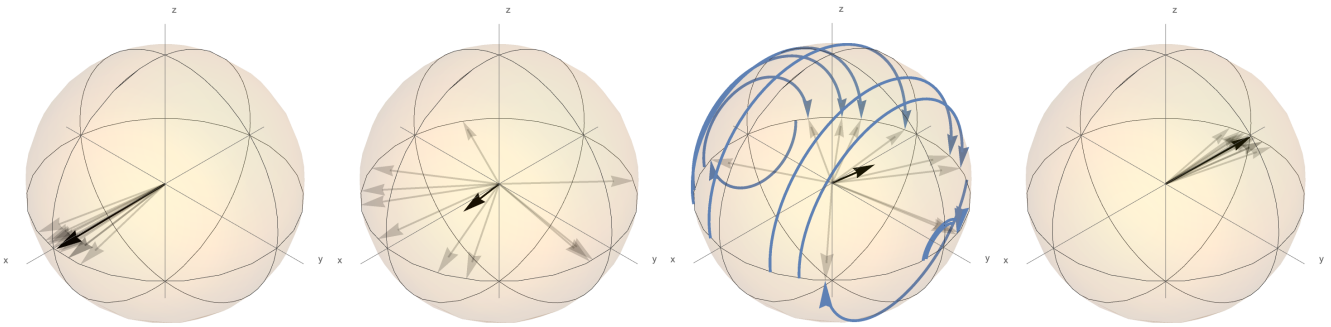

FIG. 8. Illustration of how spins (transparent vectors) dephase after a $\pi/2$ pulse, and how a π pulse can be used to reverse the dephasing process and temporarily restore the magnitude of $M_\perp$ (opaque vector) to its maximum value, referred to as a spin echo.

By applying a $\pi/2$ pulse followed by a series of π pulses, each τ seconds after the last pulse, and observing the echo amplitude, one can observe the transverse relaxation time due only to spin interactions, T_2', and not dephasing.

By removing the effect of dephasing on the relaxation of $M_\perp$, we have effectively set T_2^* to infinity in equation 5. Thus, combined with Eq. 5, Eq. 4 becomes

$$\begin{aligned} M_\perp(t) &= M_0 \left\{ \exp\left(-\frac{t}{T_2'} - \frac{t}{T_2^*} \right) \right\} \\ &= M_0 \exp\left(-\frac{t}{T_2'} \right) \end{aligned}$$

However, the effect of dephasing is only eliminated in the moment of a spin echo, which occur every τ seconds. If t_0 is taken to be the moment of the first echo, what we can measure is

$$M_\perp(t_0 + n\tau) = M_0 \exp\left(\frac{-\tau}{T_2'} \right), \qquad n \in \mathbb{N} \qquad (9)$$

Thus, in a $\pi/2, \pi$ sequence, the receiver signal was expected to show successive peaks equally spaced in time, with peak amplitude decaying exponentially over time. By equation 5, the characteristic time for the decay T_2' should be greater than T_2. It was also expected that T_2' would be shorter for rubber than for mineral oil, as motional narrowing in liquids suppresses the effects of motional narrowing [13].

The measured receiver signal is shown in Fig 9.

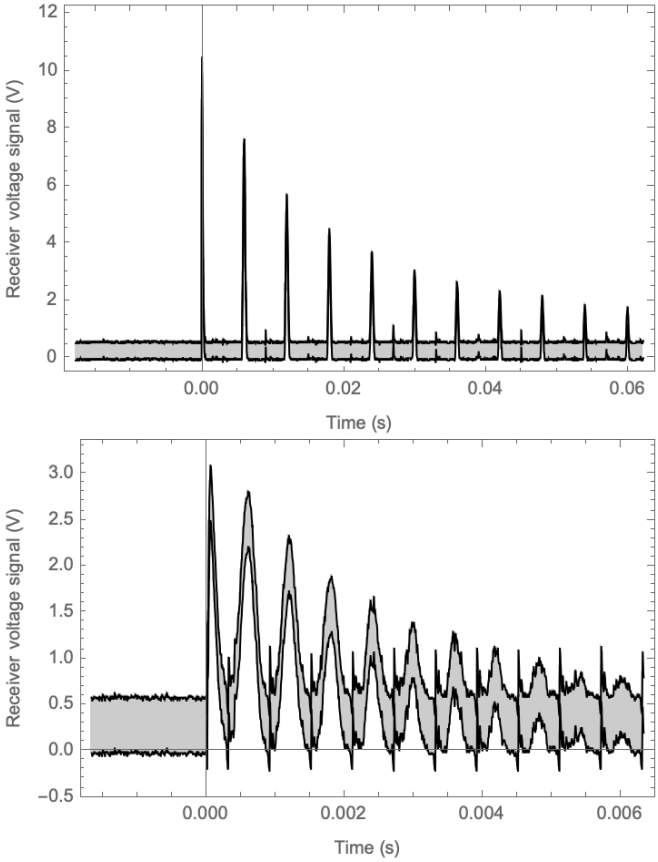

FIG. 9. Confidence interval for receiver signal after a spin echo sequence recorded for mineral oil (top) and rubber (bottom) used to calculate T_2' for the respective samples

In order to fit the raw data to Eq. 9, the echo amplitudes were extracted. The delay time τ between pulses was set on the Teachspin apparatus, which had an accuracy of $\pm 0.01ms$. The data was binned by $\tau/2$, the maximum value in each bin was found. To remove the peaks occurring between echos during the π pulses, every the maximum from every other bin was extracted, together with the number of delay times which had passed.

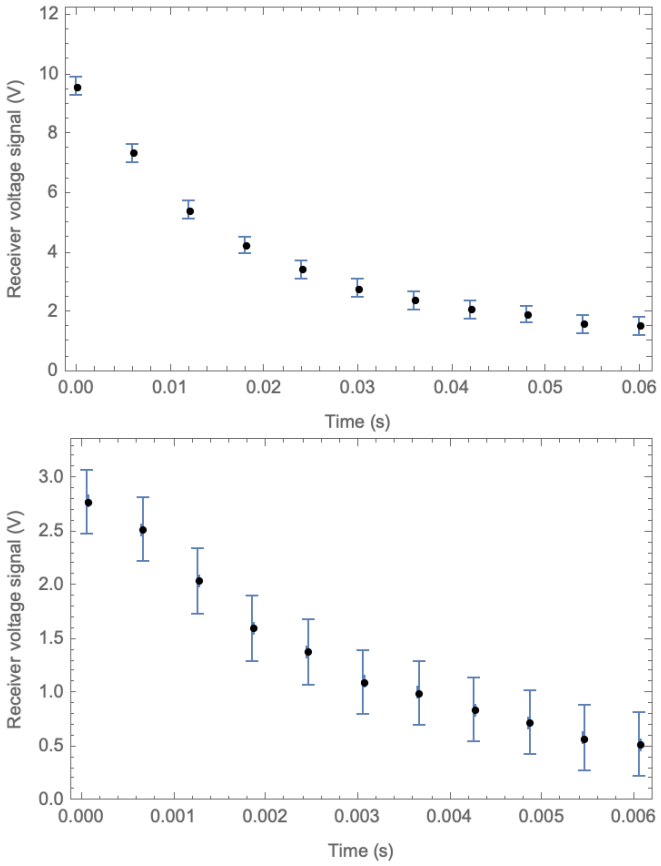

FIG. 10. Exponential decay of echo amplitude for mineral oil (top) and rubber (bottom) during a $\pi/2, \pi$ pulse sequence, used to calculate T_2' for the respective samples

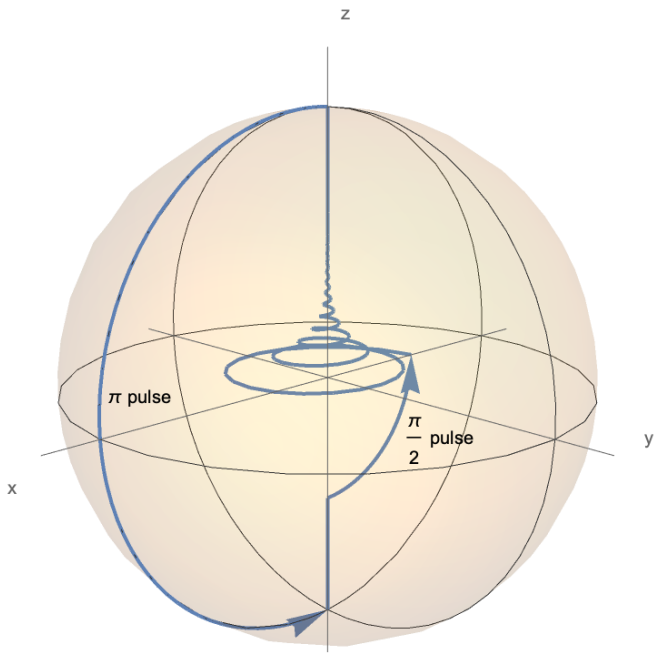

FIG. 11. Simulation of the $\pi, \pi/2$ pulse sequence for the measurement of the transverse relaxation time T_1, where the magnitude of M_z after some delay time is measured by rotating the $\vec{M}$ into the transverse plane, where it can be measured by the receiver.

As seen in Fig 10, the echo amplitude did indeed decay exponentially. In order to calculate T_2', the echo amplitude data was fitted to Eq. 9.

4. Measurement of T_1

By definition, T_1 is the characteristic time in which M_z relaxes from the south pole of the Bloch Sphere after a π pulse to its value at thermal equilibrium, M_0. In the experimental setup, the receiver can only measure the transverse component of the magnetization vector, so M_z cannot be measured directly.

When $\vec{M}$ is on the south pole of the Bloch Sphere after a π pulse, its transverse component is $M_\perp = 0$, and it remains zero throughout the decay. By applying a $\pi/2$ pulse during the decay, the magnetization vector is rotated into the transverse plane, where it undergoes FID. The amplitude of the FID signal following the $\pi/2$ pulse is the magnitude of M_z immediately before the pulse. Thus, by varying the time τ between the π and $\pi/2$ pulse and measuring the resulting FID amplitude, the relaxation of M_z was observed.

Eq. 3 is the theoretical model for $M_z(t)$ after a π pulse is applied to a sample in equilibrium. Because the receiver only measured the magnitude of M_z, the absolute value of Eq. 3 was taken when fitting the data. It was expected that, as the time delay τ between the π and $\pi/2$ pulse was increased, the FID amplitude equal to $M_z(\tau)$ would exponentially decay from its value of M_0 to 0, and then back up to approach M_0 asymptotically.

In order to measure the FID amplitude and corresponding delay time, the amplitude and location of the maximum value in the FID signal after the $\pi/2$ pulse was extracted from a single $\pi, \pi/2$ pulse sequence run. The delay time τ between pulses was set on the Teachspin apparatus, which had an accuracy of $\pm 0.01ms$. This was taken to be the uncertainty in time for each data point.

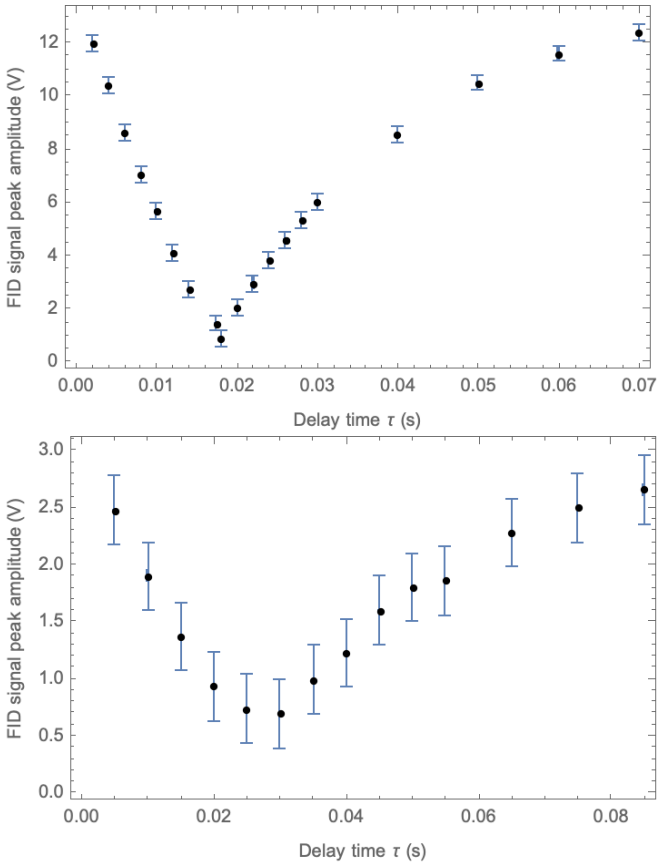

FIG. 12. Exponential decay of FID amplitude for mineral oil (top) and rubber (bottom) after a $\pi, \pi/2$ pulse sequence, used to calculate T_1 for the respective samples

As expected, the FID signal amplitude initially decreased to a minimum, after which it increased again, appearing to approach an asymptote after around .06s in the delay time.

The τ for which the FID signal amplitude was minimized was also determined up to the accuracy in time provided by the TeachSpin apparatus, $\pm 0.01ms$. This was taken to be the uncertainty in time for each data point.

$$\exp\left(-\frac{t_0}{T_1}\right) = \frac{1}{2}$$
$$t_0 = T_1 \log 2 \tag{10}$$

and this equation was used as a second way to calculate T_1.

C. Error Analysis & Error Bars

Within our measurements, there are several error bars which are collectively displayed on our graphs. These were measured by observing the variance of each data point on the oscilloscope, as there were fluctuations inherent to each measurement. As such, we redid each variance measurement for each subsequent material to ensure that there would be no overlap between materials. Additionally, we were able to find the uncertainty on the best fit point using the subsequent formula:

$$\Delta\chi^2 - \chi_{Min} = 1 \tag{11}$$

This allows us to find one standard deviation uncertainty, which is shown in our final result.

V. COMPARISON OF DATA WITH THEORETICAL MODEL

A. Calculation of T_2 from measurement

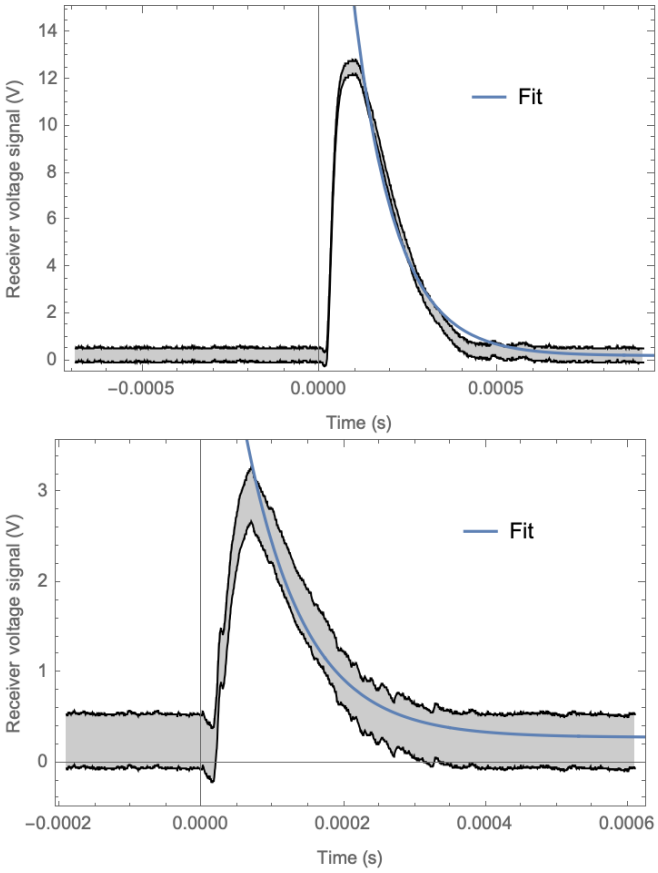

FIG. 13. Fit of Eq. 4 to the measured FID signal after a $\pi/2$ pulse for mineral oil (top) and rubber (bottom).

Material	T_2
Mineral Oil	$118 \pm 25\mu s$
Rubber	$0.1 \pm 0.1ms$

TABLE I. Calculated value of T_2 for mineral oil and rubber

As seen in Fig 13, while the exponential fit for rubber was consistent, the exponential fit for mineral oil was

not perfectly consistent with the measured signal. Especially as the signal approaches its background level, it decreases faster than the exponential function. The fit for mineral oil was more consistent with an exponential function, but even so, the graph seems approximately linear rather than exponential in the initial decrease from the maximum value.

For both rubber and mineral oil, the model of the data was adjusted from Eq. 4 to include a constant offset equal to the average background signal when no pulses are present. As seen in Fig 13, the background signal was not centered around $0V$ before and after the FID. In order to find the background signal offset, an average was taken over data with no pulses for each sample. This offset was subtracted from the data when fitting the model.

B. Calculation of T_2' from measurement

Material	T_2'
Mineral Oil	$25 \pm 4ms$
Rubber	$2.7 \pm 0.7ms$

TABLE II. Calculated value of T_2' for mineral oil and rubber

As seen in Fig 14, the exponential fit for the decay of the echo amplitudes was consistent with the data for rubber, but not perfectly consistent for mineral oil, especially as the echos approached the background signal value. Similar to the model for T_2, the model of the data was adjusted from Eq. 9 to include a constant offset equal to the average background signal.

Additionally, T_2' was shorter for mineral oil, as expected due, to the presence of motional narrowing.

C. Calculation of T_1 from measurement

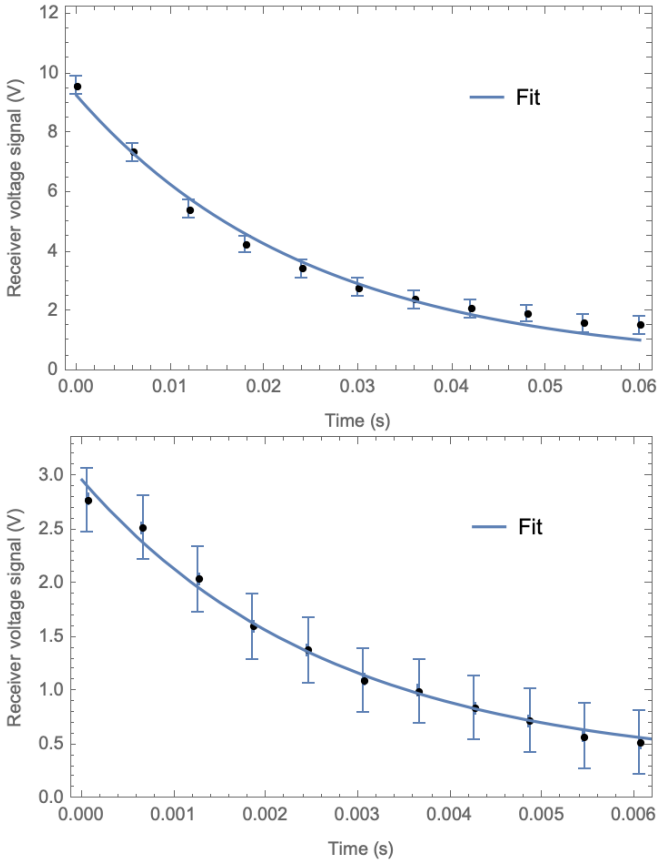

FIG. 14. Fit of Eq. 9 to the measured echo amplitudes after a $\pi/2, \pi$ pulse sequence for mineral oil (top) and rubber (bottom).

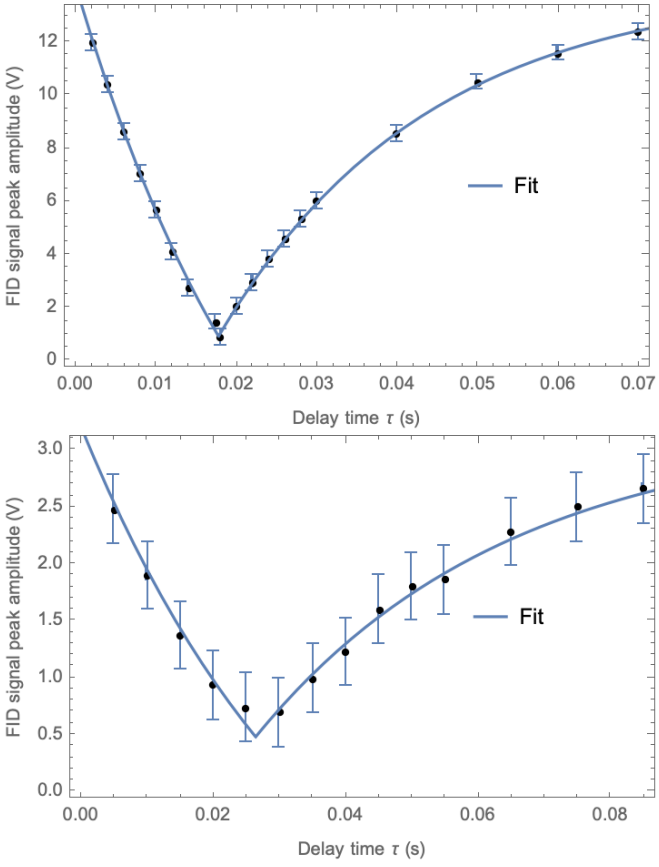

FIG. 15. Fit of Eq. 3 to the measured FID amplitudes after a $\pi, \pi/2$ pulse sequence for mineral oil (top) and rubber (bottom).

Material	T_1 from fit	T_1 from minimizing
Mineral Oil	$26 \pm 2ms$	$27.0 \pm 0.3ms$
Rubber	$38 \pm 11ms$	$43 \pm 15ms$

TABLE III. Calculated value of T_1 for mineral oil and rubber from fit and from finding the delay time corresponding to the minimum FID amplitude, related to T_1 by Eq. 10

The uncertainty in the T_1 measurement from minimizing the FID amplitude was estimating the range of delay times over which the FID amplitude appeared to be at a minimum and did not noticeably change.

As seen in Fig 15, fit of the FID amplitude to Eq. 3 was consistent for both mineral oil and rubber. However, while fitting, the average background subtracted from the data was not sufficient for a consistent fit, and an additional offset was added. This indicates the presence of some effect currently not accounted for.

D. Determination of T_2^*

From Eq. 5 and the measured values of T_2, the values of T_2^* were calculated.

Material	T_2^*
Mineral Oil	$118 \pm 36.707\mu s$
Rubber	$85.5 \pm 112\mu s$

TABLE IV. Calculated value of T_2^* for mineral oil and rubber

The uncertainty in T_2^* was calculated by adding the relative uncertainties of T_2, T_2' in quadrature.

E. Determination of reduced χ^2 with degrees of freedom

Using Eq. 7 and 8, we are able to find the reduced χ^2 value for our data vs our fit. Within the Eq. 8, the variable n is referring to the number of counts which were observed in the data set, and m is the degrees of freedom which were used in the fitting of our data. For all of our data, we had two degrees of freedom. Subsequently, we were able to find the reduced χ^2 fit for each of our data points which are in Table V.

	Reduced Chi Squared		Reduced Chi Squared
T1Oil	0.045433	T1Rub	0.0165472
T2Oil	0.409792	T2Rub	0.0357934
T2'Oil	0.0242575	T2'Rub	0.0185661

TABLE V. This table shows the values of reduced χ^2 which were obtained after plotting our evaluated data vs our observed data.

F. Form Fitting Equation and Parameters

For our fit parameters, the following equations were used in order to model how the data should behave over time. The following equations were used in order to model this. Additionally, we took a measurement of the fluctuations inherent with our sample without any pulses being sent to the sample and labelled this value as Average Background, or AvgBackground for short.

$$|M_0(1 - 2Exp\left(\frac{-t}{T1}\right) + Avg.Background)| \tag{12}$$

$$M0 * Exp[-(t - t_{MaxDataValue})/T2] + AvgBackground \tag{13}$$

$$M0 * Exp[-t/T2P] + avgBackground \tag{14}$$

From here, we were able to use an algorithm which minimized the χ^2 value of the fit until we had a best fit in accordance with the equations above.

VI. DISCUSSION AND CONCLUSION

For the data observed, a fit was established based on the Bloch equations which were used to model the position of the magnetization vector with respect to time. This fit was subsequently compared to our data using the reduced χ^2 equation with degrees of freedom.

There were several systematic errors which were found from a variety of sources. One which was particularly problematic to deal with was the resolution of the oscilloscope was only able to be focused to a certain degree. This was due to us requiring the peaks from the π and $\frac{\pi}{2}$ pulses to be visible at the same time in order to compare the decay time between them. Furthermore, it was clear that it was very easy to disrupt the system and cause random noise to be introduced into the system. This was evident in particular when a laptop charger was placed within the same room as the machine and generated a large degree of noise on the oscilloscope. Subsequently, there were the obvious limitations that come with the machines which we were working in the sense that their precision often had some intrinsic offsets (Such as the time division stating it was in 100 ms when it was 1ms). Finally, the test vial which we used was listed simply as an "oil" without specific indication to which oil it was referring to. We believe that this oil is Mineral Oil, despite us initially believing that we had tested for Glycerin. Our experimental data matches up well with the values for Mineral Oil additionally.

Subsequently, there were two main assumptions which were made while observing the data. The first was assumed that when measuring the data, our equipment was perfectly on resonance, when in reality this may not have been the case. Additionally, there was a bit of a "drift"

which was noticed in our data viewed on the oscilloscope. It had a tendency to move slightly if left on for too long. This is was most likely caused by magnetic drift, which causes a magnetic field to vary from 1-10 Hz per hour. [14]

Furthermore, we were able to compare and contrast the different values which we obtained for our values in contrast to a paper titled *NMR Techniques Applied to Mineral Oil, Water, and Ethanol* written by L. Bianchini and L. Coffey at Brandeis University [15]. In their experiment, they obtained a value for T_1 to be around 27.5 $\pm$.4ms, and we found $T_1 = 25.2 \pm 0.1ms$, inconsistent but within 5%. They found T_2 to be around 15.7 $\pm$.2 and we found $T_2 = 13.6 \pm 0.1\mu s$, also inconsistent but within 8%. As such, the values obtained in this report match up well within the generally accepted values for the spin decay times.

Finally, there were several modifications which could've been implemented in the lab for future research. One would be to enable the user to lock the frequency such that there would be no magnetic drift found in the experiment. [14]. Additionally, an oscilloscope which was able to read two distinct peaks onscreen to a higher degree of precision would've been helpful for decreasing the amount of uncertainty which was found in the lab.

[1] I. I. Rabi, Space quantization in a gyrating magnetic field, Phys. Rev. **51**, 652 (1937).

[2] F. Bloch, W. W. Hansen, and M. Packard, Nuclear induction, Phys. Rev. **69**, 127 (1946).

[3] E. M. Purcell, H. C. Torrey, and R. V. Pound, Resonance absorption by nuclear magnetic moments in a solid, Phys. Rev. **69**, 37 (1946).

[4] E. D. Becker, Analytical Chemistry **65** (1993).

[5] J. L. O'Brien, Optical quantum computing, Science 10.1126/science.1142892 (2007).

[6] P. van der Straten and H. Metcalf, *Atoms and Molecules Interacting with Light: Atomic Physics for the Laser Era* (Cambridge University Press, 2016).

[7] N. F. Ramsey, History of atomic clocks, Journal of research of the National Bureau of Standards (1977) **88**, 301 (1983).

[8] J. Roberts, *Nuclear Magnetic Resonance: Applications to Organic Chemistry* (McGraw-Hill, 1959).

[9] Nanoscale nmr spectroscopy and imaging of multiple nuclear species, Nature Nanotechnology **10**, 129 (2015).

[10] F. Bloch, Nuclear induction, Phys. Rev. **70**, 460 (1946).

[11] E. L. Hahn, Spin echoes, Phys. Rev. **80**, 580 (1950).

[12] G. Instek, *GDS-1000A-U Specifications*, Good Will Instrument Co, N0. 7-1, Jhongsing Road, Tucheng Dist., New Taipei City, 236, Taiwan (2022), a full MANUAL entry.

[13] L. Mihaly, *NMR Writeup*, Stony Brook University, 100 Nicolls Rd, Stony Brook, NY 11794 (2012), a full MANUAL entry.

[14] A. Maier, Benchtop nmr blog, Nanalysis (2021).

[15] L.Bianchini and L. Coffey, *NMR Techniques Applied to Mineral Oil, Water, and Ethanol*, M.S. thesis, Brandeis University, MA 02453.